Electronic Supplementary Material (ESI) for RSC Advances.

Supplementary Informations

Solution behavior and encapsulation properties of fatty acid-elastin-like polypeptide conjugates.

Tingting Zhang, Frédéric Peruch, Amélie Weber, Katell Bathany, Martin Fauquignon, Angela Mutschler, Christophe Schatz, Bertrand Garbay

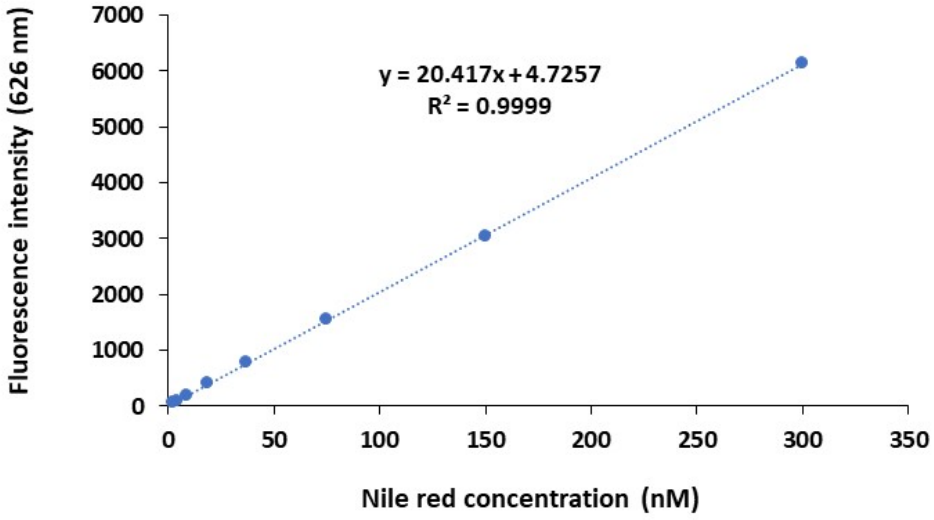

Figure S1. Calibration curve for determination of the Nile red (NR) concentration in DMSO. The mean fluorescence intensity of NR at λ_{em} = 626 nm (λ_{ex} = 550 nm) was determined for serial dilutions of a NR solution at 2 µM in DMSO.

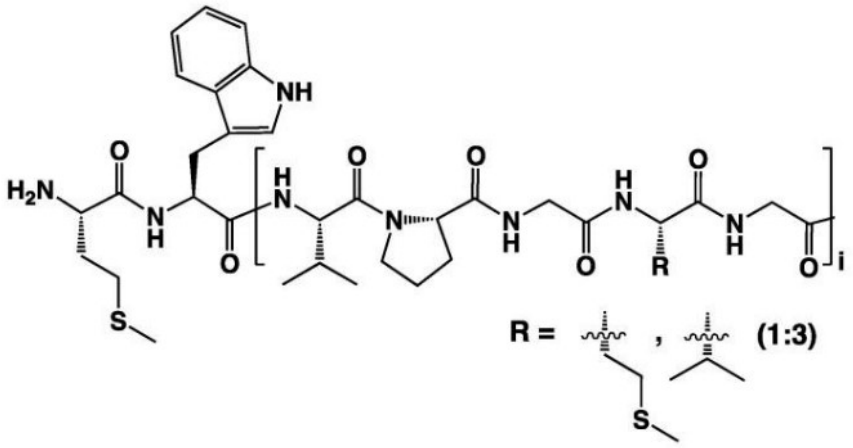

Figure S2. Chemical structure of the ELP M-series. The guest amino acid is either a methionine or a valine, with a molar ratio 1:3. The number of pentapeptide repetition (i) is 20, 40 and 80.

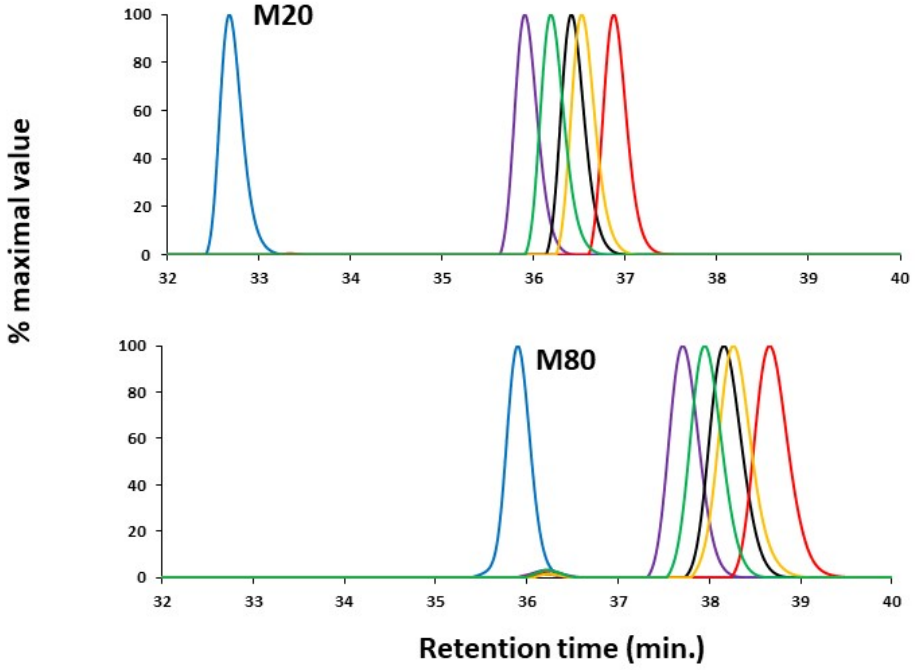

Figure S3. RP-HPLC chromatograms of M20-FAs and M80-FAs. ELP-FAs were injected at a concentration of 70 µM in water. The eluent was a gradient of a water/methanol mixture. The absorbance at 230 nm was normalized to the maximal value. Chromatograms of unmodified ELP (blue lines), ELP-C14 (purple lines), ELP-C16 (black lines), ELP-C18 (red lines), ELP-C18:1 (orange lines) and ELP-C18:2 (green lines) are plotted for the M20 and M80 series.

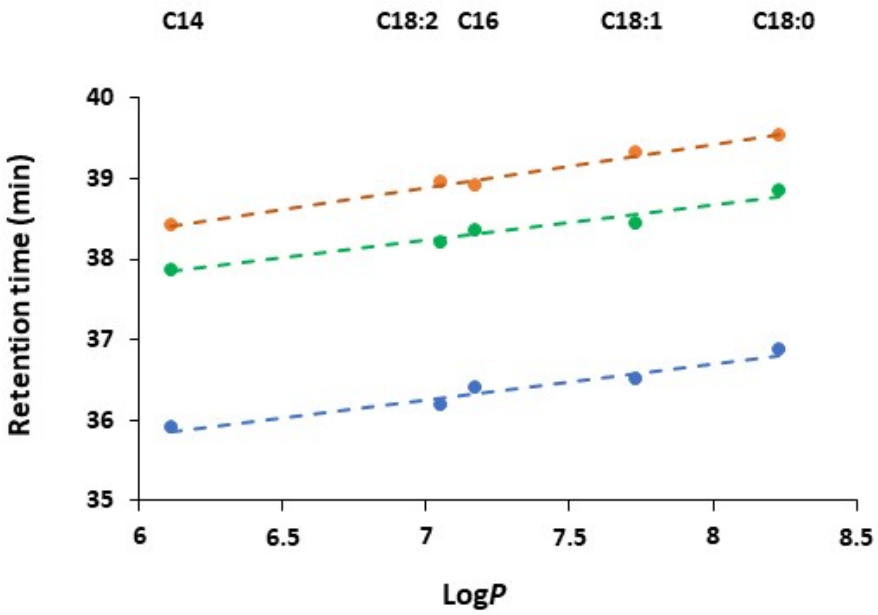

Figure S4. Retention times of ELP-FA conjugates measured by RP-HPLC as function of the Log*P* value of the fatty acids. M20-FAs (blue), M40-FAs (green) and M80-FAs (orange).

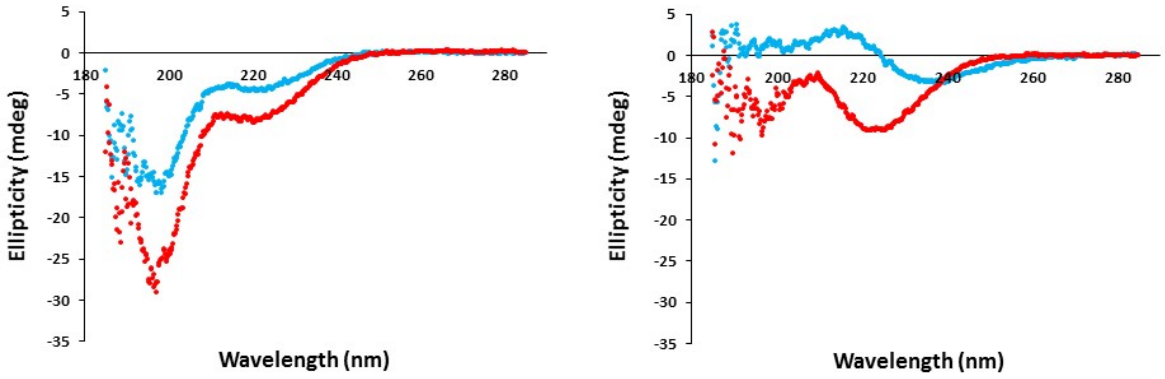

Figure S5. Circular dichroism spectra of 10 µM solutions of M80 and M80-C16 in water. The spectra were recorded at 10 °C (left side) and 50 °C (right side). Blue traces correspond to M80, red traces correspond to M80-C16.

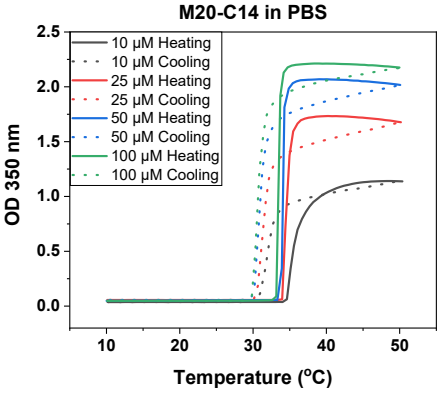
M20-C14 in PBS
10 μM Heating
10 μM Cooling
25 μM Heating
25 μM Cooling
50 μM Heating
50 μM Cooling
100 μM Heating
100 μM Cooling
OD 350 nm
Temperature (°C)

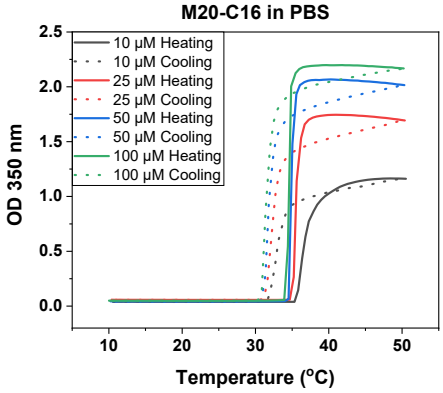
M20-C16 in PBS
10 μM Heating
10 μM Cooling
25 μM Heating
25 μM Cooling
50 μM Heating
50 μM Cooling
100 μM Heating
100 μM Cooling
OD 350 nm
Temperature (°C)

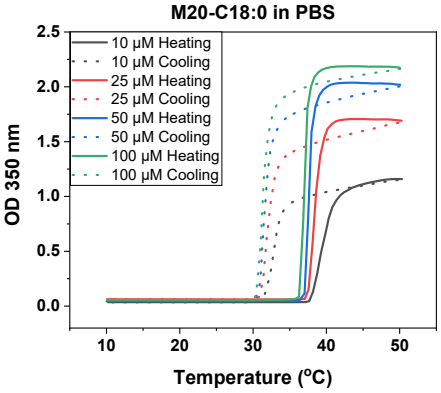
M20-C18:0 in PBS
10 μM Heating
10 μM Cooling
25 μM Heating
25 μM Cooling
50 μM Heating
50 μM Cooling
100 μM Heating
100 μM Cooling
OD 350 nm
Temperature (°C)

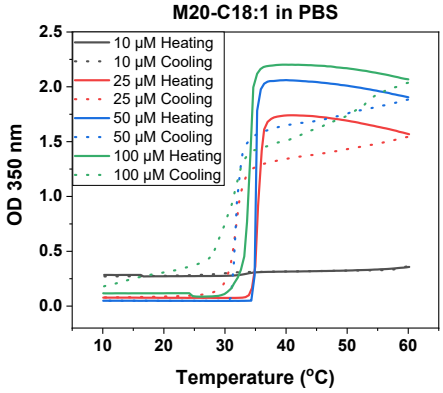
M20-C18:1 in PBS
10 μM Heating
10 μM Cooling
25 μM Heating
25 μM Cooling
50 μM Heating
50 μM Cooling
100 μM Heating
100 μM Cooling
OD 350 nm
Temperature (°C)

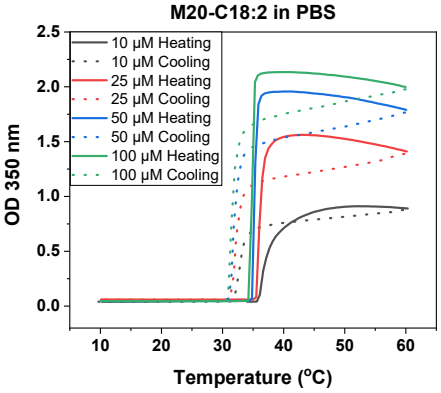
M20-C18:2 in PBS
10 μM Heating
10 μM Cooling
25 μM Heating
25 μM Cooling
50 μM Heating
50 μM Cooling
100 μM Heating
100 μM Cooling
OD 350 nm
Temperature (°C)

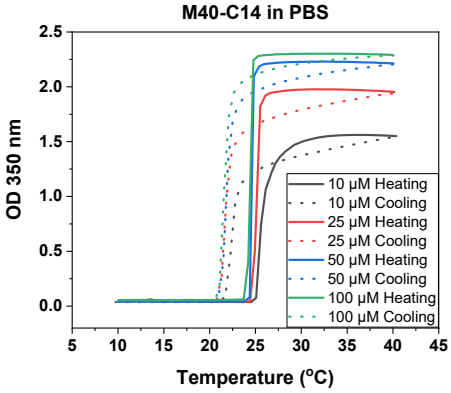
M40-C14 in PBS
10 μM Heating
10 μM Cooling
25 μM Heating
25 μM Cooling
50 μM Heating
50 μM Cooling
100 μM Heating
100 μM Cooling
OD 350 nm
Temperature (°C)

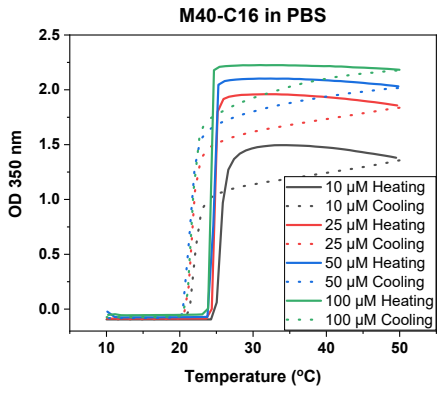
M40-C16 in PBS
10 μM Heating
10 μM Cooling
25 μM Heating
25 μM Cooling
50 μM Heating
50 μM Cooling
100 μM Heating
100 μM Cooling
OD 350 nm
Temperature (°C)

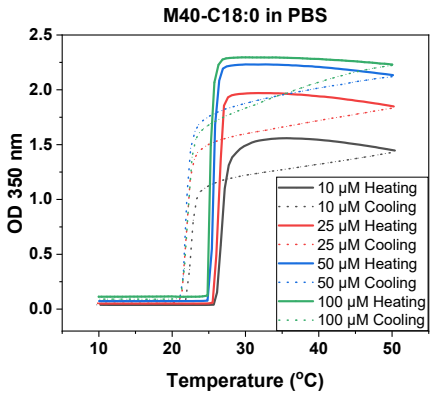
M40-C18:0 in PBS
10 μM Heating
10 μM Cooling
25 μM Heating
25 μM Cooling
50 μM Heating
50 μM Cooling
100 μM Heating
100 μM Cooling
OD 350 nm
Temperature (°C)

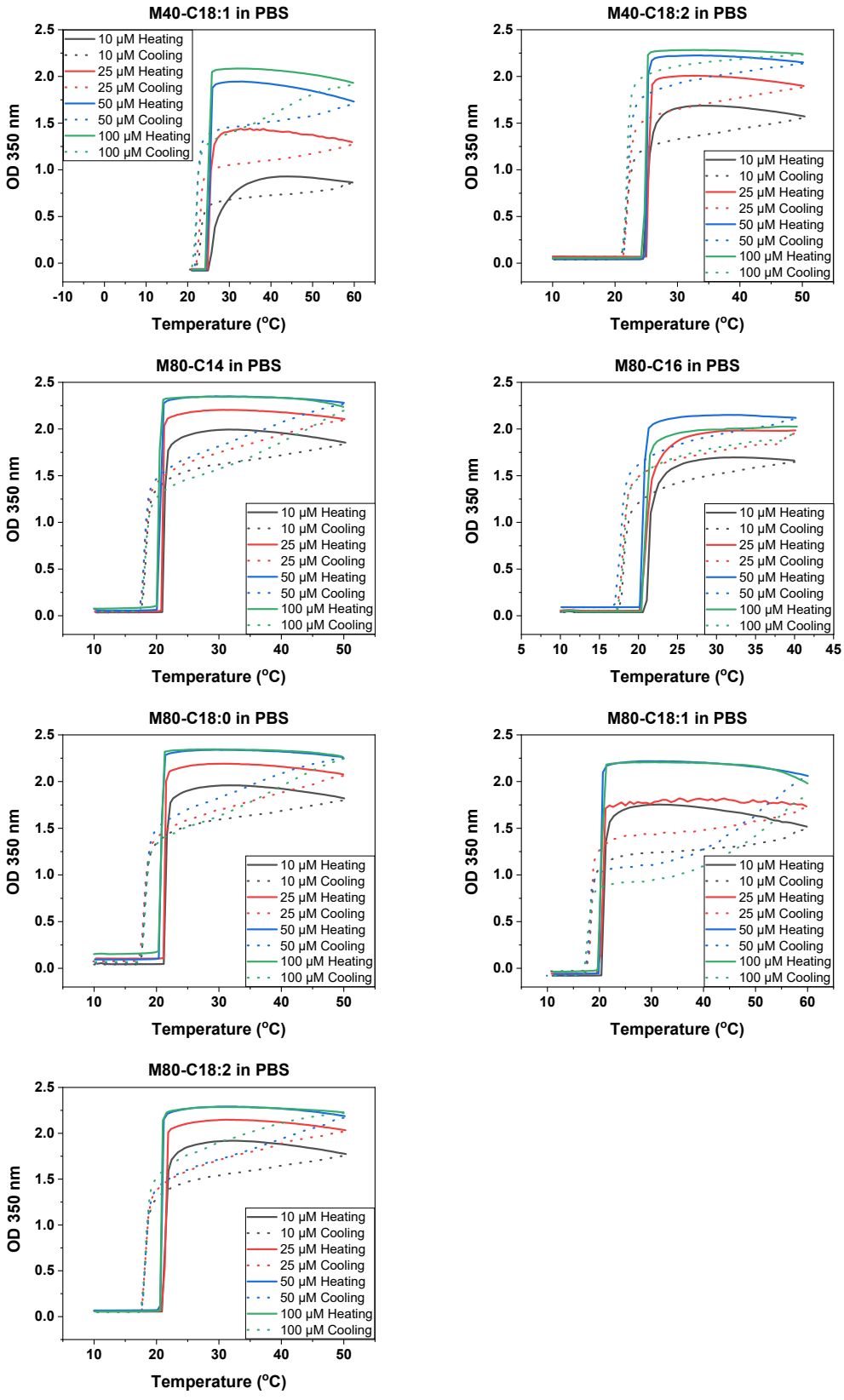

Figure S6. T-scans of the 15 ELP-FAs at various concentrations in PBS. Heating ramps

(plain lines) and cooling ramps (dashed lines) are given at various conjugate concentrations, from 10 µM to 100 µM. The absorbances of the solutions were recorded at 350 nm.

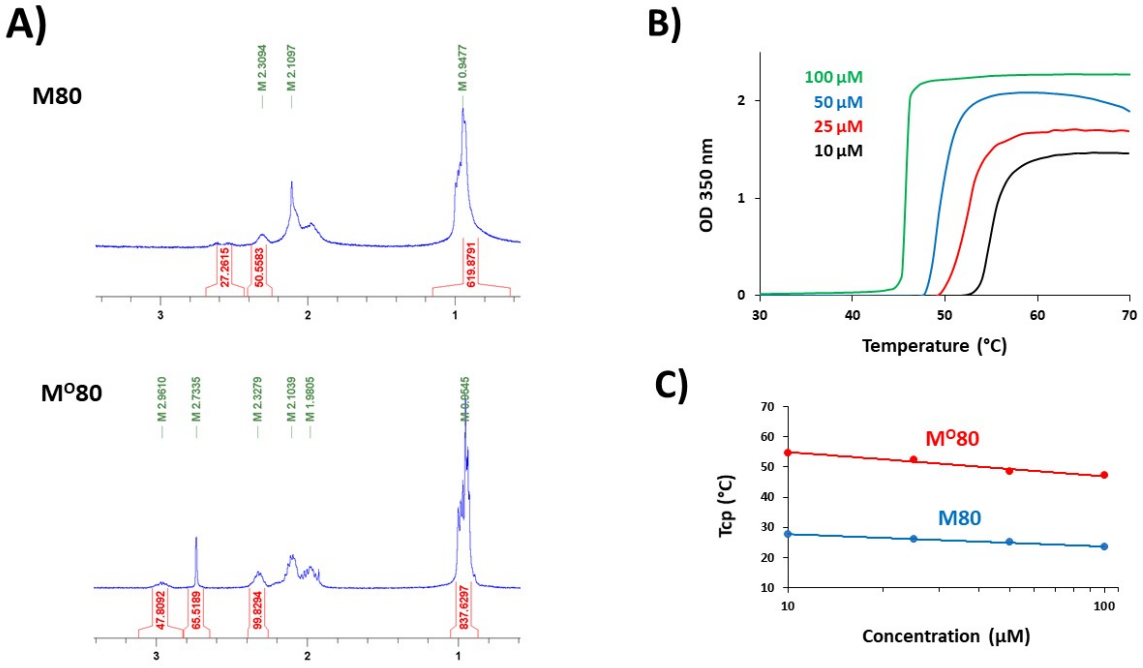

Figure S7. Characterization of the oxydized M80. A) ^{1}H NMR analysis of M80 (Top) and M^{O}80 (bottom). The apparition of a characteristic peak corresponding to the sulfoxide function can be detected at 2.73 ppm[1]. The integration of this peak indicates that 95% of the methionine were oxidized **B)** Turbidimetry experiments with different concentrations of M^{O}80 in PBS buffer. **C)** Tcp values of M80 and M^{O}80 as function of the ELP concentrations. Tcps values of M^{O}80 are about twice as high as those of the M80.

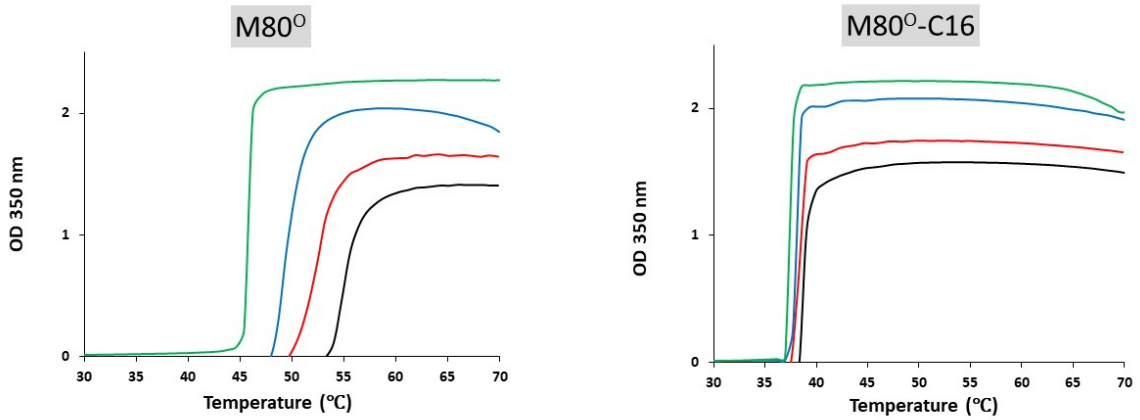

Figure S8. T-scans of M^{O}80 and M^{O}80-C16 at various concentrations in PBS. Only the heating steps are plotted.

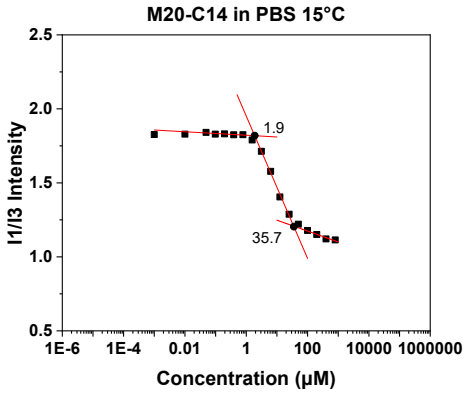
M20-C14 in PBS 15°C
I1/I3 Intensity
Concentration (μM)
1.9
35.7

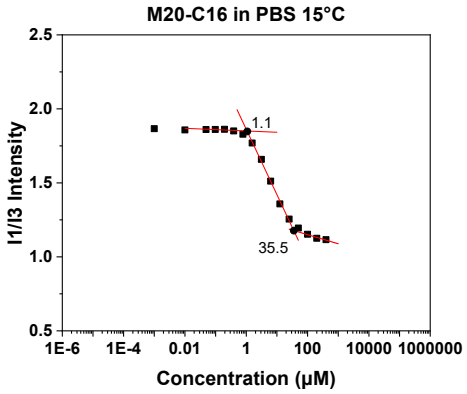
M20-C16 in PBS 15°C
I1/I3 Intensity
Concentration (μM)
1.1
35.5

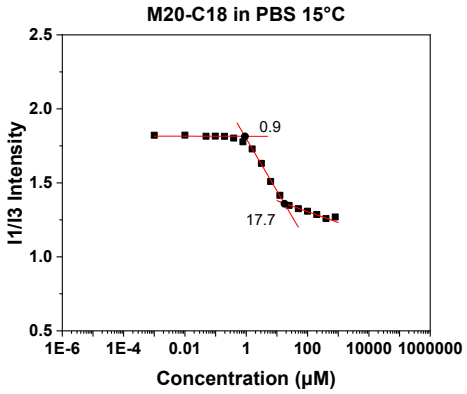
M20-C18 in PBS 15°C
I1/I3 Intensity
Concentration (μM)
0.9
17.7

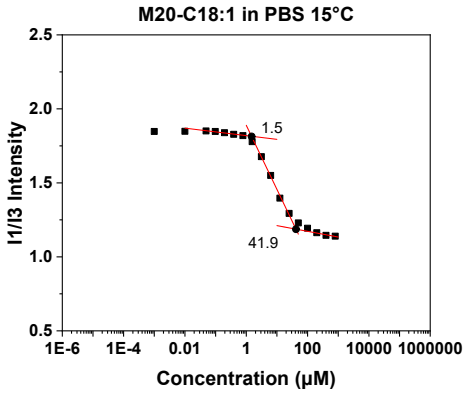
M20-C18:1 in PBS 15°C
I1/I3 Intensity
Concentration (μM)
1.5
41.9

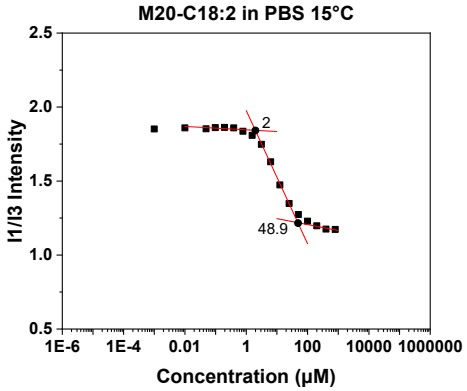
M20-C18:2 in PBS 15°C
I1/I3 Intensity
Concentration (μM)
2
48.9

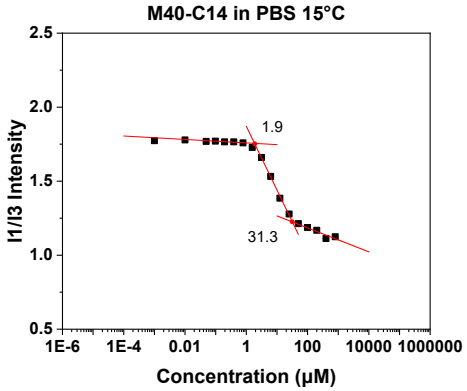
M40-C14 in PBS 15°C
I1/I3 Intensity
Concentration (μM)
1.9
31.3

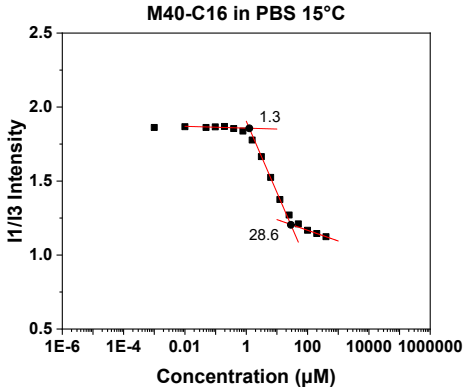
M40-C16 in PBS 15°C
I1/I3 Intensity
Concentration (μM)
1.3
28.6

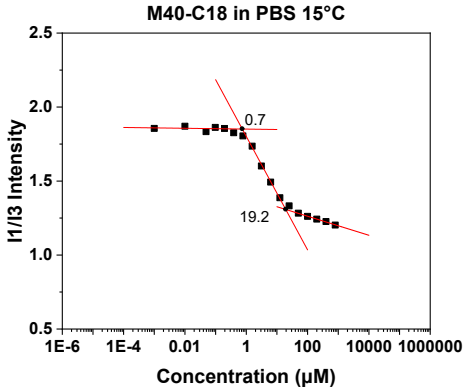
M40-C18 in PBS 15°C
I1/I3 Intensity
Concentration (μM)
0.7
19.2

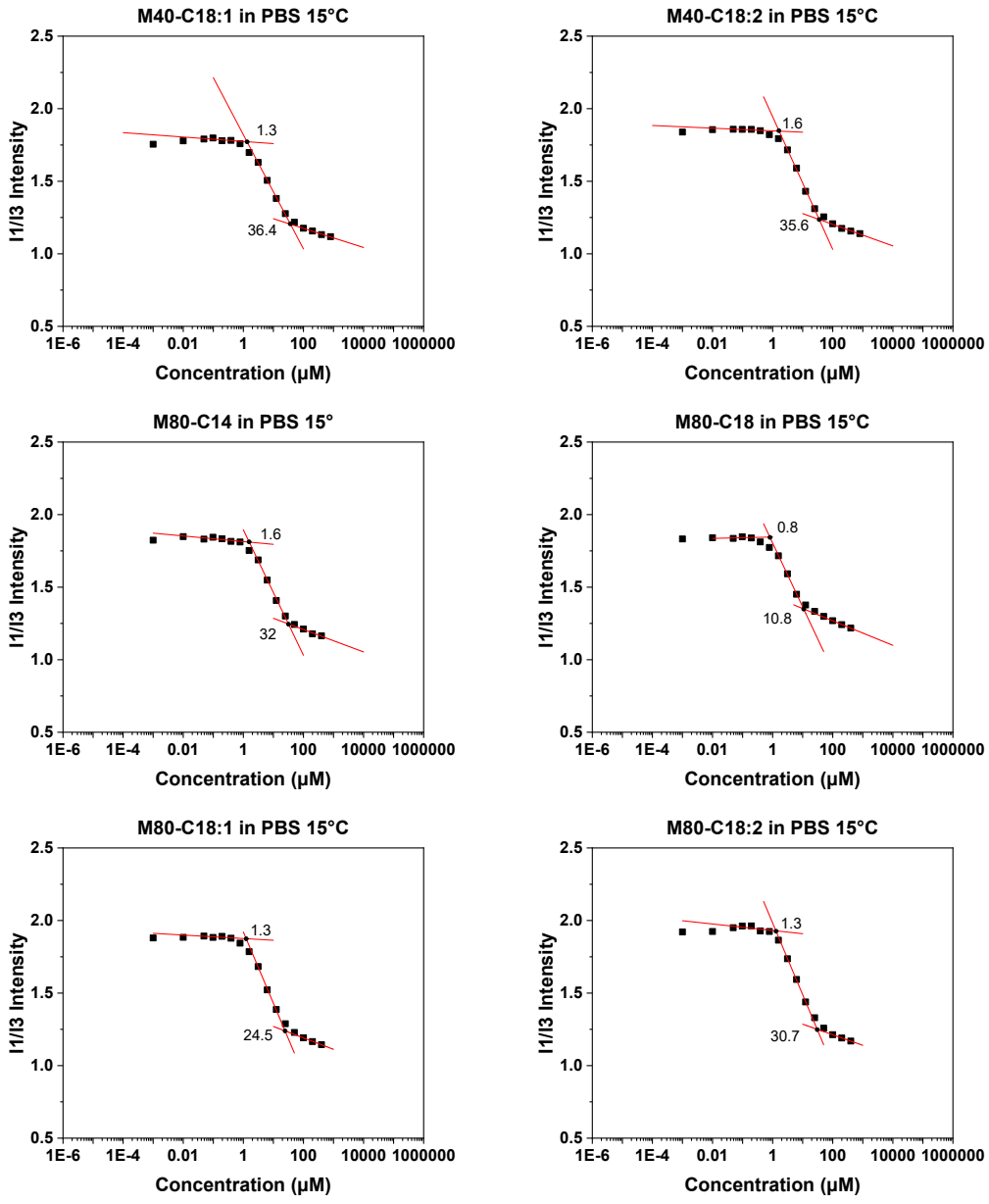

Figure S9. Variation of the I1/I3 ratio for ELP-FAs in PBS at 15°C as function of the conjugate concentration. The CMC values shown on the graphs correspond to the "low" and "high" CMC values (see Fig. 3.A).

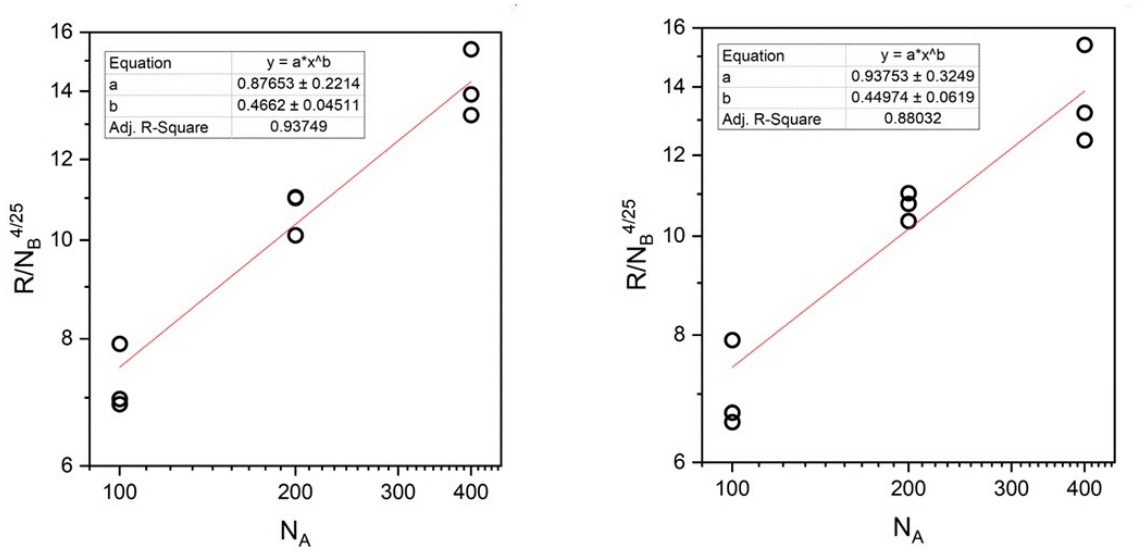

Figure S10. **Fitting analysis of ELP-FA micelles with a star model**. The micelle radii determined by the cumulant analysis of DLS data were fitted with a modified scaling law proposed by Halperin[2], $R \sim N_B^{4/25} N_A^{\nu}$ with N_B and N_A the degree polymerization of the FA and ELP blocks. *Left* : data obtained with C14, C16, C18; *Right* : data obtained with C18, C18:1, C18:2.

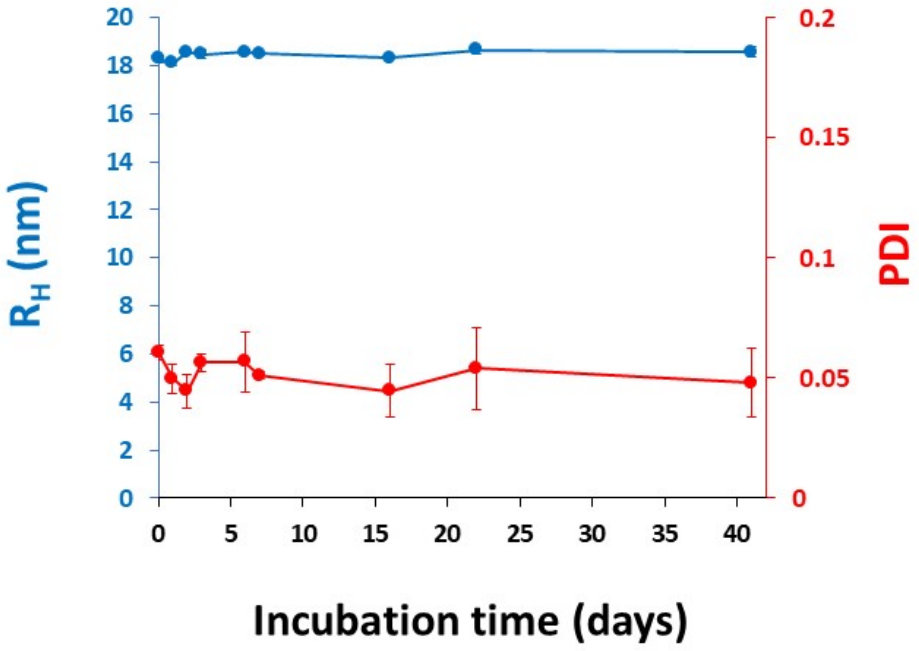

Figure S11. Stability of M80-C16 nanoparticles upon storage at 4°C in PBS buffer. M80-C16 was solubilized into PBS at a concentration of 5 mg mL^{-1} (147 µM). The sample was stored at 4 °C, and R_H (nm) and PDI were recorded at 15 °C. For each value, data are mean of three measures ± SD.

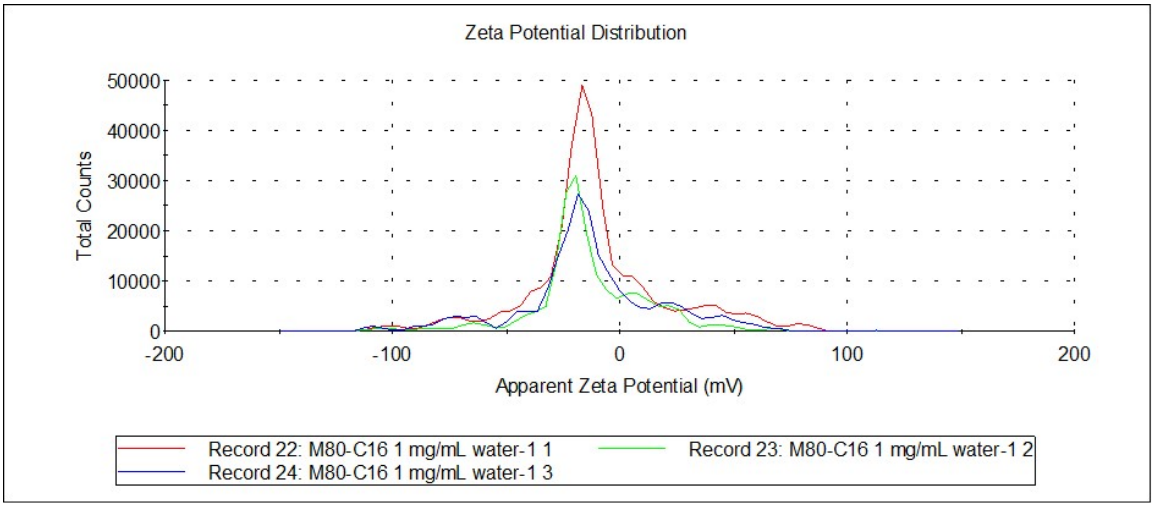

Figure S12. Zeta potential distribution of M80-C16 micelles in water at 1 mg mL^{-1}.

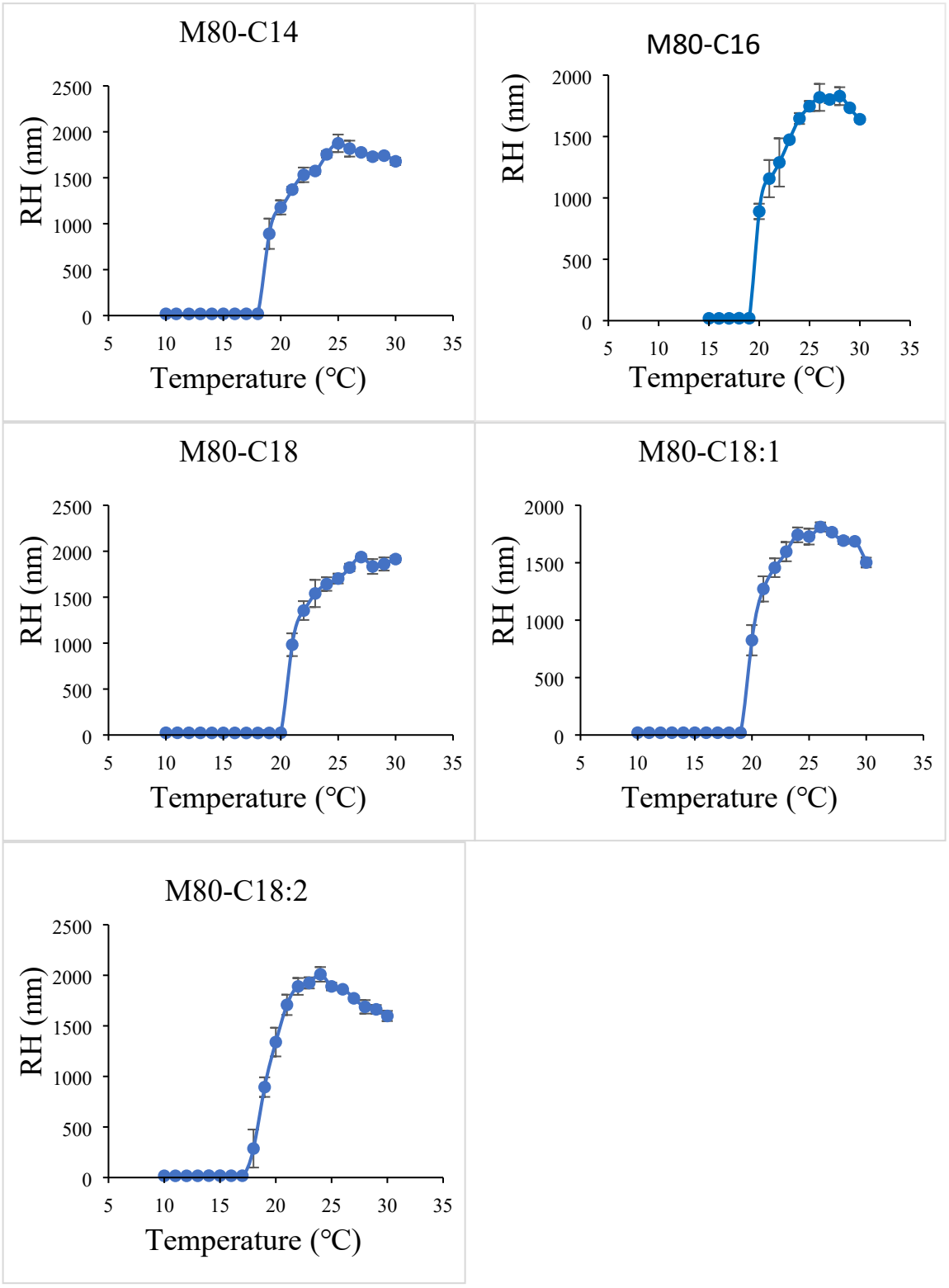

Figure S13: Variation of the hydrodynamic radius of ELP-FA micelles during a temperature ramp. Solutions of M80-C14, M80-C16, M80-C18, M80-C18:1 and M80-C18:2 at a concentration of 1 mg mL^{-1} in PBS buffer were analyzed by DLS between 10 and 30 °C. For each value, data are mean of three measurements ± SD.

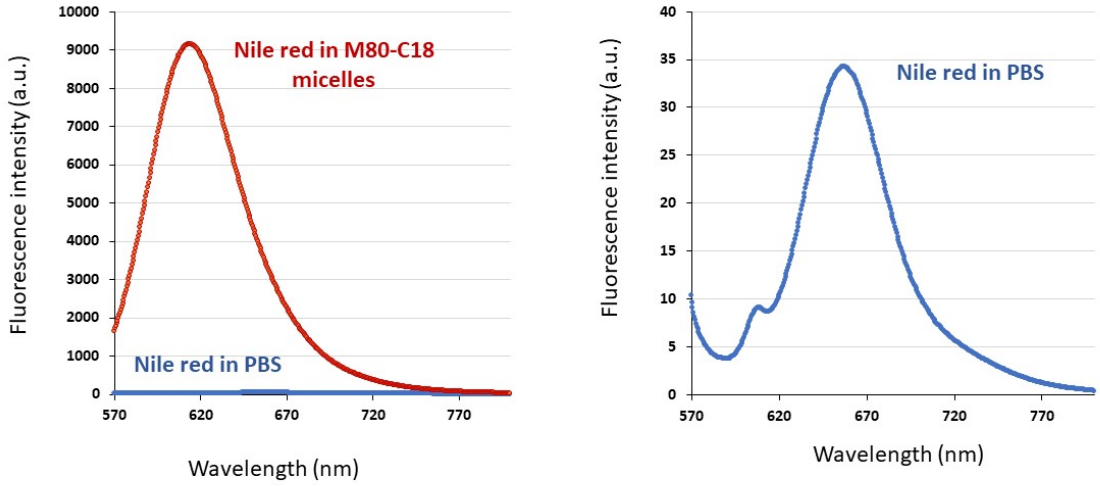

Figure S14: Nile red fluorescence in PBS and after encapsulation in M80-C18 micelles.
2 µl of a 3 mM solution of Nile red in DMSO were mixed with either 600 µL of PBS (blue traces) or 600 µL of a solution of M80-C18 at 1 mg mL^{-1} in PBS (red traces). The fluorescence of the two samples was recorded between 570 nm and 780 nm.

Table S1. Gradient program used for analytical RP-HPLC

Buffer A: Water + 0.1% TFA
Buffer B: Methanol + 0.1% TFA

Time (min)	% buffer A	% buffer B
0	100	0
3	100	0
35	0	100
45	0	100
46	100	0
55	100	0

Table S2. Physico-chemical characteristics of the fatty acids used in the study.

Fatty acid	Common Name	MW (g mole^{-1})	Log P	Melting Point (°C)
C14:0	Myristic acid	228.4	6.11	53.9
C16:0	Palmitic acid	256.4	7.17	61.8
C18:0	Stearic acid	284.5	8.23	68.8
C18:1	Oleic acid	282.5	7.73	13.4
C18:2	Linoleic acid	280.4	7.05	-8.5

Table S3. Targeted ELP-FA conjugates.

		C14		C16		C18		C18:1		C18:2	
	[a]MW	MW	[b]ELP:FA	MW	ELP:FA	MW	ELP:FA	MW	ELP:FA	MW	ELP:FA
M20	8 687	8 897	38.1 :1	8 925	33.9 :1	8 953	30.5 :1	8 951	30.8 :1	8 949	31.0 :1
M40	17 035	17 245	74.7 :1	17 274	66.5 :1	17 301	59.9 :1	17 300	60.4 :1	17 298	60.8 :1
M80	33 735	33 945	148.0 :1	33 974	131.8 :1	34 002	118.8 :1	34 000	119.6 :1	33 998	120.5 :1

[a.]theoretical molecular weight in g mole^{-1}. Data for ELP were obtained from ProtParam[3].
[b.]ELP/FA: mass ratio

Table S4. RP-HPLC analysis of ELP-FAs

		ELP	ELP-C14	ELP-C16	ELP-C18	ELP-C18:1	ELP-C18:2
M20	[a]Retention time	32.7	35.9	36.4	36.9	36.5	36.2
	[b]Purity (%)		99	99	99	99	99
M40	Retention time	35.3	37.9	38.4	38.9	38.5	38.1
	Purity (%)		96	99	98	98	96
M80	Retention time	35.9	37.7	38.2	38.7	38.3	37.9
	Purity (%)		96	97	97	98	96

[a.]retention times in min.
[b]purity was determined from the peak area of ELP-FA relative to the total peak area on the same chromatogram

Table S5. Molecular weight of ELP and ELP-FAs samples measured by ESI-MS

ELP and ELP-FA	Theoretical MW (g mole^{-1})	Expérimental MW (g mole^{-1})
M20	8 687	8 686
M20-C14	8 897	8 896
M20-C16	8 925	8 924
M20-C18	8 953	8 952
M20-C18:1	8 951	8 950
M20-C18:2	8 949	8 948
M40	17 035	17 037
M40-C14	17 246	17 246
M40-C16	17 274	17 274
M40-C18	17 302	17 302
M40-C18:1	17 300	17 300
M40-C18:2	17 298	17 298
M80	33 736	33 739
M80-C14	33 946	33 946
M80-C16	33 974	33 973
M80-C18	34 002	34 002
M80-C18:1	34 000	34 000
M80-C18:2	33 998	33 998

Table S6. Tcp values (in °C) of ELP-FA conjugates at different concentrations in PBS.

	concentrations	C14	C16	C18	C18:1	C18:2
M20	100 µM	33.2	34.4	36.8	34.2	34.8
	50 µM	33.9	34.5	37.5	34.9	34.8
	25 µM	34.0	35.2	38.1	35.0	35.2
	10 µM	34.6	35.8	38.8	33.5	36.1
M40	100 µM	24.2	23.9	24.8	24.2	24.7
	50 µM	24.4	24.6	25.4	25.1	24.9
	25 µM	25.0	24.4	26.0	24.8	25.0
	10 µM	25.1	25.0	27.7	26.5	24.5
M80	100 µM	20.0	20.4	20.3	19.7	20.5
	50 µM	20.1	20.2	20.4	19.9	20.6
	25 µM	20.8	20.7	21.1	20.3	20.8
	10 µM	20.9	21.1	21.2	20.4	20.9

Table S7. High (H) and low (L) CMC values (in µM) in PBS at 15 °C for the 15 ELP-FAs studied.

	C14		C16		C18		C18:1		C18:2	
	L	H	L	H	L	H	L	H	L	H
M20	1.9	36	1.1	36	0.9	18	1.5	42	2.0	49
M40	1.9	31	1.3	29	0.7	19	1.3	36	1.6	36
M80	1.6	32	0.9	26	0.8	11	1.3	24	1.3	30

Table S8. R_H (nm) and PDI values of ELP-FA micelles in PBS measured by DLS at 15 °C

		ELP-C14	ELP-C16	ELP-C18	ELP-C18:1	ELP-C18:2
M20-fatty acid	R_H	9	9	11	9	9
	PDI	0.029	0.030	0.022	0.054	0.018
M40-fatty acid	R_H	13	14	15	14	14
	PDI	0.104	0.188	0.012	0.134	0.172
M80-fatty acid	R_H	17	18	21	18	17
	PDI	0.074	0.116	0.075	0.080	0.046

Table S9. Values of the rate constant (k), release exponent (n), and correlation coefficient (R^2) determined from the the Korsmeyer-Peppas equation ($Qt/Q_\infty = kt^n$) for M80-FA micelles.

	k	n	R^2
M80-C14	1.52	0.74	0.998
M80-C16	2.18	0.64	0.999
M80-C18	0.45	0.79	0.998

Bibliography

1 R. Petitdemange, E. Garanger, L. Bataille, W. Dieryck, K. Bathany, B. Garbay, T. J. Deming and S. Lecommandoux, *Biomacromolecules*, 2017, **18**, 544–550.

2 A. Halperin, *Macromolecules*, 1987, **20**, 2943–2946.

3 E. Gasteiger, C. Hoogland, A. Gattiker, S. Duvaud, M. R. Wilkins, R. D. Appel and A. Bairoch, *The Proteomics Protocols Handbook*, 2005, **112**, 571–607.